RESEARCH ARTICLE

Studying the structure and optical properties of FeCl₃: ITO prepared by sol–gel dip coating technique

Alaa M. Theban[1] · Falah H. Ali[1] · Asmaa J. Kadhim[2]

© The Author(s), under exclusive licence to The Optical Society of India 2024

Abstract This work used the sol–gel dip coating process to generate thin films of pure indium tin oxide and indium tin oxide film mixing with FeCl₃ at ratios of 50, 100, and 150%. Indium and tin precursors, such as InCl₃ and SnCl₄, were affordable. The produced ITO samples were examined by UV–Vis, SEM, XRD, EDX, and AFM spectroscopy. The primary peak of the (222) plane, according to the thin film XRD patterns, matched a high degree of crystallinity in indium oxide. The elements In, O, Sn, Fe, and Cl are present in the deposited layers, according to the EDX spectrum. According to the SEM pictures, the average diameter of the particles for pure, 50, 100, and 150% were 23.87, 41.12, and 36.27 nm, respectively. From AFM images, the average grain size of pure ITO film was 61 nm. The films with different ratios 50, 100, and 150% had average grain sizes of 96, 36, and 178 nm respectively. The optical band gap of pure ITO was 4.49 eV, while for films ITO + FeCl₃ with different mixing ratios 50, 100, and 150% the energy gap was 2.61, 2.89 and 2.35eV, respectively. From the contact angle found the water contact angles 32.57°, 18.74°, 73.66°, and 43.98° for pure, 50, 100, and 150%, respectively are apparent. It can be found that the contact angle decreases at mixing ratios of 50%, this result indicates that the hydrophilicity of ITO surface at low mixing ratios, this a behavior is due to the reduction of surface roughness.

✉ Falah H. Ali
f58280812@gmail.com

1 Department of Physics, College of Science, University of Baghdad, Baghdad, Iraq

2 Department of Physics, College of Science for Woman, University of Baghdad, Baghdad, Iraq

Introduction

Because of its rare combination of conducting and transparent qualities, indium tin oxide (ITO) has become a significant engineering material. In the optoelectronic industry, ITO thin films have been the subject of much research. ITO thin film is an extremely degenerate n-type semiconductor with a $(2.4) \times 10^{-4}$ Ω.cm electrical sheet resistance [1–6]. The Fermi level (EF) is above the conduction level (EC), which results in a high carrier concentration and a low resistivity value of ITO films. High conductivity ITO sheets have a carrier concentration between 10^{20} and 10^{21} cm^{-3}. ITO films also feature high transmittance, high reflectance in the IR range, good electrical conductivity, great substrate adhesion, and hardness. This is because ITO is a broadband gap semiconductor (*Eg*: 3.5–4.3 eV) [7–15]. These layers are frequently utilized in many different applications, including heatable devices, sensors, solar cells, electrochromic devices, displays, and more. Sputtering, spray pyrolysis, pulsed laser deposition (PLD) [16–18], thermal evaporation, screen printing, and sol–gel are the most often utilized techniques for ITO deposition [15–23]. Usually, following deposition, these films are annealed to produce high-quality ITO films. The study of colloidal particles or monolithic structures of metal oxides resulting from the hydrolysis and subsequent condensation of metal alkoxides or salts is known as sol–gel science. The process of changing from a solution to a gel like phase is basically implied by the phrase "sol–gel," which accurately characterizes the process by which metal oxides are formed from metal alkoxides. The sol–gel approach offers several benefits, this technique makes it simple to manage the dopant amount and solution density, as well as to coat the desired shapes and areas [24]. Moreover, in

contrast to other approaches, the procedure is simple and does not require the use of costly or sophisticated equipment. By adjusting the firing and annealing temperatures or the atmosphere in which the annealing is done, the electrical and optical properties of ITO films can be altered. This also impacts the densification and crystallization of the ITO films [25–27]. Generally speaking, the annealing process and microstructure optimization lead to the production of free electrons or oxygen vacancies, which reduce an ITO film's resistivity [10]. ITO thin films were created in the current study using a straightforward and affordable sol–gel dip coating method. A thorough investigation was conducted on the impact of $FeCl_3$ on the characteristics of ITO.

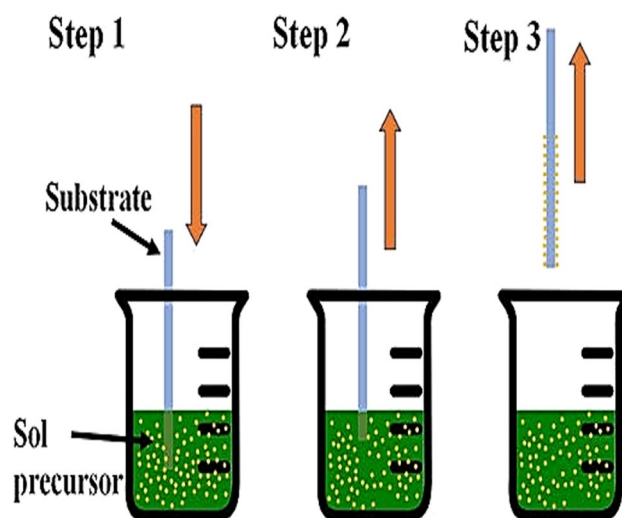## Experimental work

Preparation of ITO

50 ml of double-distilled water were used to dissolve 1.1727g of $InCl_3$ and 0.1402g of $SnCl_4$, which served as precursors for the creation of ITO. After both solutions were let to sit at room temperature for 30min on a magnetic stirrer, they were combined in a 100ml glass container and stirred continuously for 120min. To finish the reaction, little drops of NaOH were carefully added to the mixture [10]. The solution's PH was nine. After 15min at 4000rpm in the centrifuge, the final solution had the same amount of ethanol added and the water removed using a burette. Then dried for 2h at 500 ^{o}C in the oven for preparation [28]. $FeCl_3$:ITO,

Fig. 2 Shows the dip coating method

three different weights of $FeCl_3$, 0.0975, 0.195, and 0.2925g were combined with 10 ml of ethanol and left to dissolve at room temperature for 30 min on a magnetic stirrer. These solutions were combined to 10 ml of ITO to obtain mixing ratios 50, 100, and 150%. Figure 1, depicts pure ITO solution and ITO with different mixing ratios of $FeCl_3$ 50, 100, and 150%.

Preparation of ITO film and contact angle measurement

Pure ITO films and $FeCl_3$:ITO films with varying ratios 50, 100, and 150% was prepared by repeating the heat treatment

Fig. 1 Shows from left; pure ITO solution and ITO with different mixing ratios of $FeCl_3$, 50, 100, and 150% respectively

Fig. 3 Contact angle measuring experimental setup

Fig. 4 XRD of samples: **a** pure film, **b** ratio 50%, **c** ratio100% and **d** ratio150%
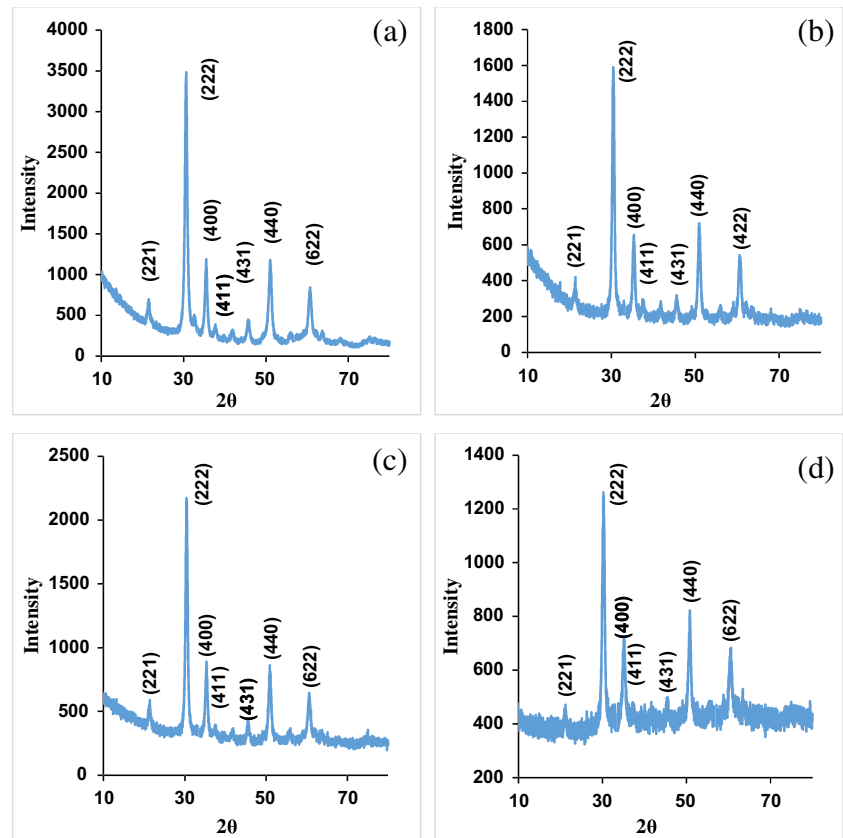
and dip coating processes. As seen in Fig. 2, dip coating is an easy, inexpensive, dependable, and repeatable process that includes immersing the substrate in a solution to deposit a wet liquid film [28, 29]. Numerous factors, including immersion duration, concentration, withdrawal speed, number of dipping cycles, temperature, solution composition, concentration, humidity level in the environment, etc., affect the film's characteristics and thickness and thickness was measured by Shererr equation. In this work the silica glass was dipped in 20 ml of solution three times and each time the layer dried at 80°C for 10 min. The thickness of synthesized samples are 85, 95, and 105 nm respectively.

Using a contact angle apparatus depicted in Fig. 3, the hydrophilic behavior of a water droplet on the films was assessed. Using a micro-injector (5 µl) syringe aimed vertically down into the sample surface, a water droplet is injected onto the film's surface. A macro lens on a high-resolution camera takes a picture of the water droplet. These images are analyzed using analytic software [30].

Result and discussion

The crystal structures of pure ITO powder and ITO powder with FeCl$_3$ at varying ratios 50, 100, and 150% in the range 10°-80° are studied using X-ray diffraction patterns. XRD

Table 1 Summary of XRD results for all samples

| Sample	2θ (deg)	FWHM(deg)	d(A)	(hkl)	D(nm)
Pure ITO	21.6	0.10	16.35	(211)	27.0
	30.5	0.30	11.65	(222)	20.6
	35.4	0.20	10.07	(400)	81.0
	37.9	0.20	9.43	(411)	84.1
	45.8	0.20	7.87	(431)	43.2
	51.8	0.20	7.017	(440)	22.0
	60.9	0.30	6.04	(622)	30.7
ITO + FeCl$_3$ 50%	21.3	0.10	16.58	(211)	81.0
	30.4	0.30	11.68	(222)	27.5
	35.3	0.20	10.10	(400)	40.5
	37.7	0.18	9.48	(411)	46.7
	45.7	0.15	7.89	(431)	57.5
	51.0	0.20	7.11	(440)	44.0
	60.7	0.20	6.06	(622)	46.1
ITO + FeCl$_3$ 100%	21.4	0.1	16.50	(211)	81.0
	30.4	0.25	11.68	(222)	33.0
	35.3	0.25	10.10	(400)	32.4
	37.6	0.09	9.50	(411)	93.4
	45.7	0.15	7.89	(431)	57.5
	51.0	0.28	7.11	(440)	31
	60.6	0.25	6.07	(622)	36.8
ITO + FeCl$_3$ 150%	21.2	0.09	16.65	(211)	90
	30.3	0.2	11.72	(222)	41.2
	35.1	0.25	10.16	(400)	32.4
	37.5	0.09	9.53	(411)	93.4
	45.5	0.15	7.92	(431)	57.5
	50.7	0.2	7.15	(440)	44.2
	60.0	0.16	6.13	(622)	57.6

patterns for pure samples and samples with varying mixing ratios are displayed in Fig. 4a, d. As can be observed, all of the films are polycrystalline in character and have a predominant (222) peak in their cubic crystal structure (JCPDS: 71–2194) [9, 31–35]. The XRD results of samples show no peak corresponding to any iron or iron oxide compound, this indicates the iron diffuses interstitially in ITO thus a decrease of intensity at the different mixing ratios 50,100 and 150%.

The preferred orientation of the growth is still along the (222) plane. A slight variation in the 2θ value. The XRD analysis confirms that ITO was successfully synthesized using the sol–gel method. Crystallite size calculated using the Scherrer formula (Eq. 1) [36–38]:

$$D = \frac{K\lambda}{\beta.\cos\theta} \tag{1}$$

where K is 0.9, λ *is x-ray wavelength* 0.154 nm, β is the full-width at half maximum intensity (FWHM) measured in radian, and θ represents Bragg's diffraction angle [39]. The average crystallites sizes were 44.1, 49.0, 52.2, and 59.5 nm for pure, 50, 100, and 150% respectively. Table 1, shows the results of the XRD of all samples.

To examine the components in a sample, an analytical technique known as energy-dispersive X-ray spectroscopy (EDX) is utilized. The prepared thin films' EDX spectra, which comprise pure ITO film and ITO with different $FeCl_3$ 50, 100, and 150% mixing ratios, are shown in Fig. 5a-d.
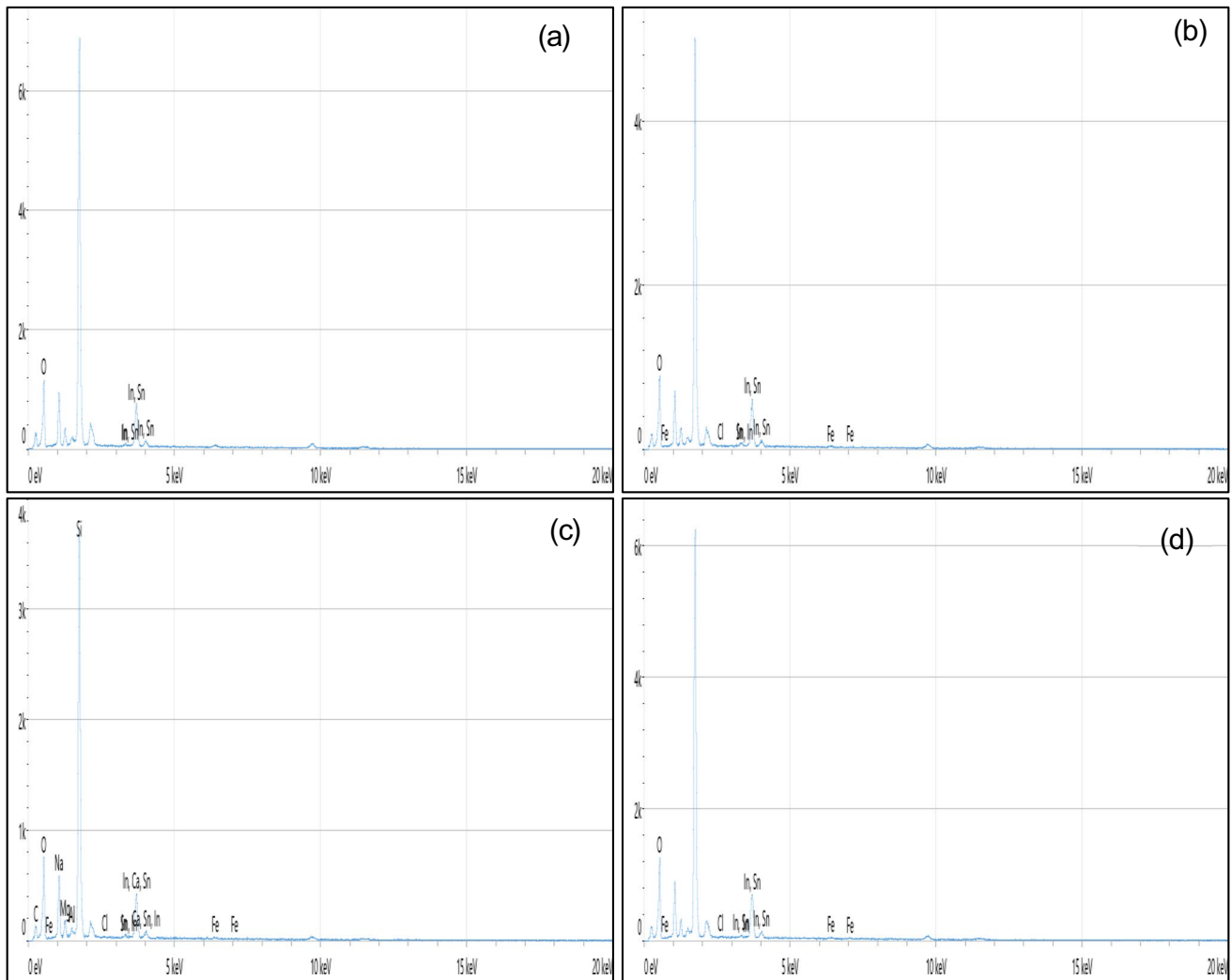
Fig. 5 EDX of samples: **a** pure film, **b** ratio 50%, **c** ratio100% and **d** ratio150%

Table 2 Summary of EDX results for all samples

Pure—Element	Atomic %	Weight %
O	96.9	81.1
In	1.3	7.9
Sn	1.8	11.0
Different mixing ratios		
ITO + FeCl$_3$ (50%)		
Cl	0.1	0.1
O	47.8	38.1
Fe	0.1	0.3
In	0.0	0.2
Sn	0.0	0.1
ITO + FeCl$_3$ (100%)		
O	96.4	80.0
Cl	0.1	0.1
Fe	0.5	1.5
In	1.4	8.4
Sn	1.6	10.0
ITO + FeCl$_3$ (150%)		
O	97.2	85.2
Cl	0.2	0.4
Fe	0.6	2.0
In	0.6	3.9
Sn	1.3	8.4

The spectra indicate that the formed coatings contain components such as In, O, Sn, Fe, and Cl and that the amount of oxygen on their surfaces has significantly increased. The weight values and atomic percentages for the films (ITO and ITO + FeCl$_3$ (50,100, and 150%)) are displayed in Table 2. Since the EDX analysis identified the presence of Fe atoms in the ITO film's structure, the lack of Fe peaks in the XRD pattern indicates that Fe atoms blended into the ITO structure. Due to the presence of some impurities, this leads to their appearance in the EDX spectrum.

One kind of electron microscope that uses a high-energy electron beam swept in a raster pattern to capture images of a sample surface is (FE-SEM). The surface morphology of thin films is determined by the parameters of the deposition process. The surface shape may have an impact on the film's mechanical, electrical, and optical properties. Figure 6a-d shows scanning electron microscopy images of pure ITO film and ITO film coated on glass substrates using the dip coating procedure at different FeCl$_3$: ITO mixing ratios 50, 100, and 150%. Figure 6a, shows that while the particles in the pure film have a variety of sizes and shapes, the majority of them have a cubic average diameter of 62.48 nm.

However, some agglomerates are several micrometers in size. whereas the ITO films had varying FeCl$_3$ ratios (50, 100, and 150 percent). It is evident that every film has a consistent surface morphology with a majority of cube-shaped particles that are well-uniform and free of cavities and fissures. The electrical conductivity and optical transmittance are enhanced by the larger active surface and reduced grain boundary. Particles with average sizes of 23.87, 41.12, and 36.27 nm were observed in the samples.

Figure 7a-d shows the AFM images of the pure ITO film and FeCl$_3$:ITO films with different mixing ratios of FeCl$_3$(50,100 and150%) deposited on a glass substrate by dip coating method over the scan area of 5.23 × 5.23, 15.9 × 15.9, 3.24 × 3.24 and 20 × 20 µm respectively. From these images, it is clear that the pure ITO film reveals the growth in the form of pointed peaks distribution over the surface of an average grain size 61 nm and root mean square height of 10.72nm, while the films with different ratios, the grains gather in the form of convex peaks and peaks with highly oriented needles-like shapes for the ratio 100% with average grain sizes 96, 36, and 178 nm respectively, while root means square height 10.13, 15.15, and 57.07nm respectively. The largest value of grain size was at the mixing ratio (150%), which may be due to the improvement of the crystalline structure and the entry of iron atoms into the places that were vacant in the crystal lattice of the (ITO) films. It was observed in the work that there is somewhat similarity in the measurement of the grain size in the results of (XRD, AFM and FESEM).

A UV–Vis spectro-photometer was used to characterize the optical property. The optical transmission of pure ITO and ITO with varying FeCl$_3$ mixing ratios in the wavelength range of 250 nm to 1100 nm is displayed in Fig. 8. It was found that for every sample the transmittance spectra increase with wavelength. FeCl$_3$ mixed with ITO has a lower optical transmittance than pure ITO. It is noticed that the transmittance decreases with the increase in the percentage of FeCl$_3$, where the added percentage of FeCl$_3$works to increase the absorbance and this is attributed to the density of the local levels formed by the added material between the valence band and the conduction band. This decrease in transmission may be due can be related to the effect of grain size. By increasing the percentage of FeCl$_3$, the grain size increases (as in the XRD results), which causes light scattering [40, 41]. ITO:FeCl$_3$ maximum optical transmittance values in the infrared range were 98% for samples with a ratio of 50%, 87% for samples with a ratio of 100%, and 93% for samples with a ratio of 150%. Notably, the samples can satisfy
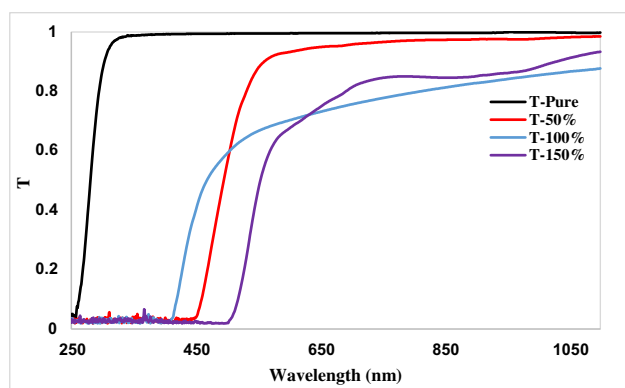
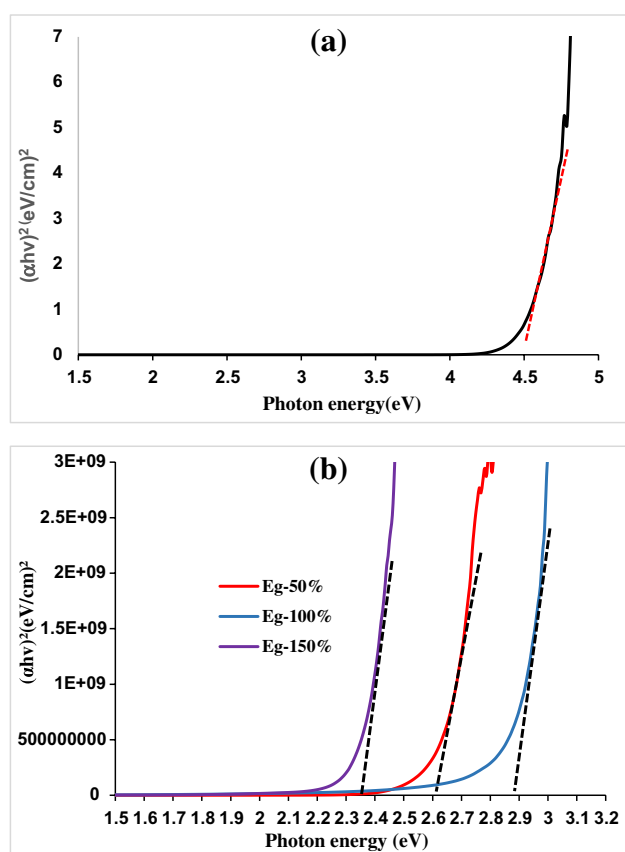**Fig. 6** Images of SEM of samples: **a** pure film, **b** ratio 50%, **c** ratio 100%, and **d** ratio 150%
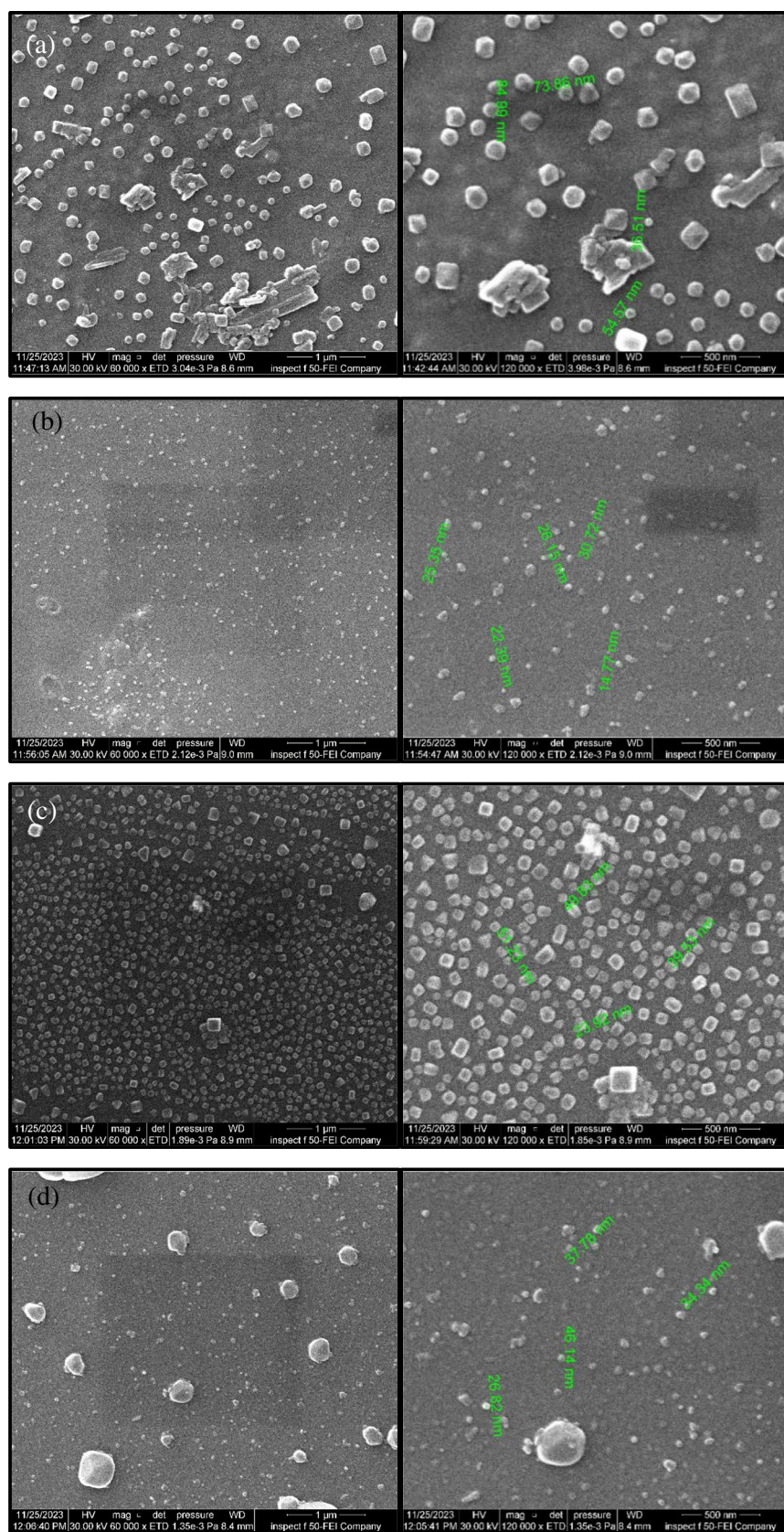
Fig. 7 Images of AFM of samples: **a** pure film, **b** ratio 50%, **c** ratio 100%, and **d** ratio 150%

(a)

(b)

(c)

(d)
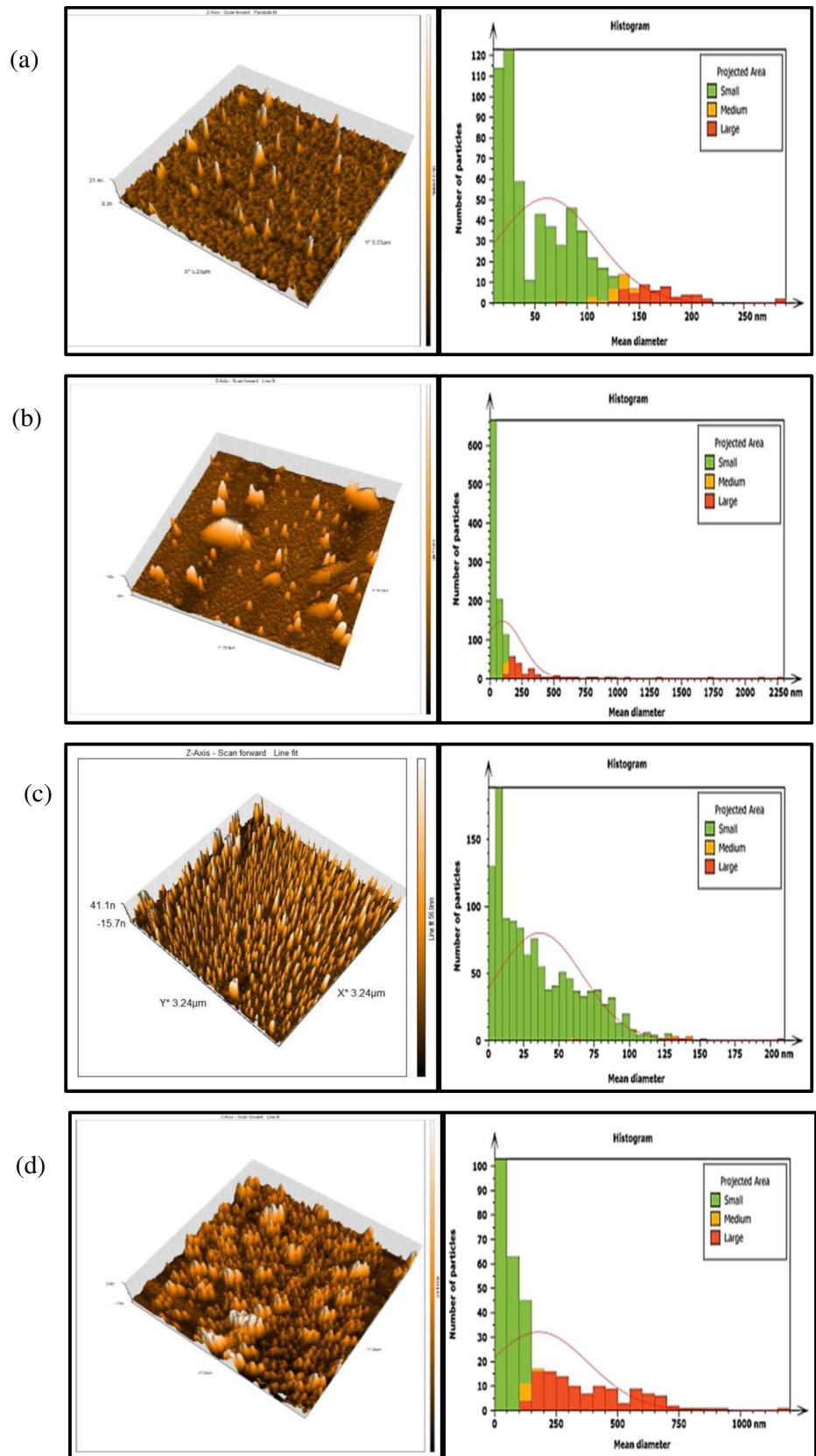
Fig. 8 Transmission spectra of pure sample and samples with different mixing ratio (50,100 and 150%)

Fig. 9 Shows Tauc's relation to determine of energy gap for (**a**) pure sample and (**b**) samples with different mixing ratios (50%,100%, and 150%)

the needs of the majority of photoelectric devices due to their great transparency in the visible and infrared regions. The thickness of synthesized samples are 85, 95, and 105 nm respectively. Figure 8, illustrate three region: the first

for represent low transmission (high absorption) (less than 250nm), second represent rapid rise range (400-600nm) and third region represent stable transmittance value (more than 600nm).

Figure 9a, b, shows the direct band gap of pure ITO and ITO with various FeCl₃ mixing ratios. This was obtained by utilizing Tauc's model to rely on the intercept of the $(\alpha h v)^2$ versus photon energy (hv) plot [41, 42].

$$\alpha h v = A\left(h v - E_g\right)^n \tag{2}$$

where α is the coefficient of absorption, ν is the frequency of incident light, A is constant, Eg is the energy band gap of material and m equals to 1/2 for direct semiconductors [43, 44]. The direct band gap of pure ITO and ITO with different mixing ratios of FeCl₃ determined using the intercept of $(\alpha h v)^2$ versus photon energy (hv) plot relying on Tauc's model [39]. The energy band gap of pure ITO was (4.49) eV [45, 46], while ITO different mixing ratios of FeCl₃ 50%,100% and 150% the energy gap was 2.61, 2.89 and 2.35eV respectively. It notice the samples at mixing ratios of 50 and 150% led to a decrease in the value of the energy gap, while the energy gap of 100% increases may be due to an aggregation [47]. This can be attributed to that these mixing ratios produce levels in the gap due to the fusion of Fe atoms with energy levels close to the edge of the beam, which may contribute to creating a gap the band is narrow, and the reason may be due to changes in the composition due to the presence of Fe atoms.

The angle between a tangent to the liquid surface and the solid surface at this point is known as the contact angle. Depending on the physical characteristics of the substance under investigation, the contact angle may be large or small. The contact angles of water on pure ITO film and ITO + FeCl₃ films with varying mixing ratios are displayed in Fig. 10a–d, where the contact angle is represented by θ. The sample 50% had the least contact angle < 18 among the pure, 50%, 100%, and 150% water contact angles, which were 32.57°, 18.74°, 73.66°, and 43.98°, respectively. This sample's surface was entirely moist. It is evident that the film's catalytic activity is correlated with the hydrophilicity at the contact angle where the angles are the shortest. Contributing to increased hydrophilicity, this finding suggests that the ITO surface's hydrophilic qualities at low mixing ratios are caused by a decrease in surface roughness [48–55].

Conclusions

Using the sol–gel process, transparent conducting ITO thin films were successfully produced. We looked into how the FeCl₃ mixing ratios affected the ITO's characteristics. We

Fig. 10 Images of water droplet on ITO and ITO + FeCl₃ surface: **a** pure film, **b** ratio 50%, **c** ratio 100% and **d** ratio 150%
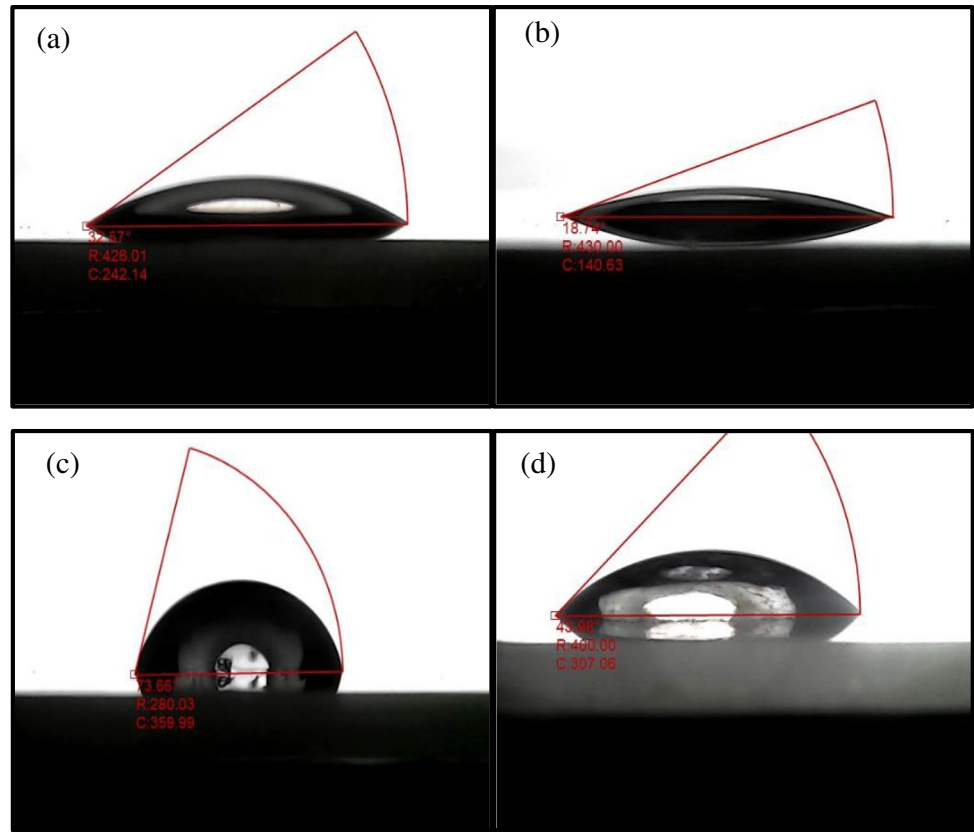
draw the conclusion that, in addition to being useful for optoelectronic applications, ITO thin films can also be prepared for use as transparent conductive electrodes in a variety of applications such as solar cells and for self-cleaning purposes. The sol–gel dip coating method works well for creating high-quality, homogeneous thin films.

References

1. H. Zhang, F. Ye, L. Liu, H. Xu, C. Sun, Synthesis of indium tin oxide nanotubes using 2-methoxyethanol as solvent via simple template method. J. Alloy. Compd. **504**(1), 171–176 (2010)
2. A.V. Moholkar, S.M. Pawar, K.Y. Rajpure, V. Ganesan, C.H. Bhosale, Effect of precursor concentration on the properties of ITO thin films. J. Alloy. Compd. **464**, 387–392 (2008)
3. L. Kerkache, A. Layadi, A. Mosser, Effect of oxygen partial pressure on the structural and optical properties of DC sputtered ITO thin films. J. Alloy. Compd. **485**(1), 46–50 (2009)
4. S.J. Hong, J.I. Han, Indium tin oxide (ITO) thin film fabricated by indium-tin-organic sol including ITO nanoparticle. Curr. Appl. Phys. **6**, 1(3), e206-e210 (2006)
5. P. Psuja, W. Strek, Fabrication of indium tin oxide (ITO) thin films by spin-coating deposition method, Proc. of SPIE, Proceedings Thin-Film Coatings for Optical Applications IV, vol. 6674, (2007) p. 667408. https://doi.org/10.1117/12.735714
6. M. Nisha, S. Anusha, A. Antony, R. Manoj, M.K. Jayaraj, Effect of substrate temperature on the growth of ITO thin films. Appl. Surf. Sci. **252**(5), 1430–1435 (2005)
7. V.G. Kytin, V.A. Kulbachinskii, O.V. Reukova, Y.M. Galperin, T.H. Johansen, S. Diplas, A.G. Ulyashin, Conducting properties of In2O3: Sn thin films at low temperatures. Appl. Phys. A **114**(3), 957–964 (2014)
8. N.M. Ahmed, F.A. Sabah, H.I. Abdulgafour, A. Alsadig, A. Sulieman, M. Alkhoaryef, The effect of post-annealing temperature on the grain size of indium-tin-oxide for optical and electrical properties improvement. Results Phys. **13**, 102159 (2019)
9. N. Vieiraa, E. Fernandesa, A. Queirozb, F. Guimarãesa, V. Zucolottoa, Indium tin oxide synthesized by a low cost route as SEGFET pH sensor. Mater. Res. **16**(5), 1156–1160 (2013)
10. M.J. Alam, D.C. Cameron, Optical and electrical properties of transparent conductive ITO thin films deposited by sol-gel process. Thin Solid Films **377–378**, 455–459 (2000)
11. M.J. Alam, D.C. Cameron, Optical and electrical properties of transparent conductive ITO thin films deposited by sol-gel process. Thin Solid Films **377–378**(6), 455–459 (2000)
12. K. Maki, N. Komiya, A. Suzuki, Fabrication of thin films of ITO by aerosol CVD. Thin Solid Films **445**(2), 224–243 (2003)
13. J.H. Kim, K.A. Jeon, G.H. Kim, S.Y. Lee, Electrical, structural, and optical properties of ITO thin films prepared at room temperature by pulsed laser deposition. Appl. Surf. Sci. **252**(13), 4834–4837 (2006)
14. K. Qian, X. Han, H. Li, T. Chen, P.S. Lee, Uncovering the indium flament revolution in transparent bipolar ITO/SiOx/ITO resistive switching memories. ACS Appl. Mater. Interfaces **12**(4), 4579–4585 (2020)

15. Y. Lin et al., 17% Efficient organic solar cells based on liquid exfoliated WS2 as a replacement for PEDOT: PSS. Adv. Mater. **31**(46), e1902965 (2019)

16. S.K. Mustafa, R.K. Jamal, K.A. Aadim, Studying the effect of annealing on optical and structure properties of ZnO nanostructure prepared by laser induced plasma. Iraqi J. Sci. **60**(10), 2168–2176 (2019)

17. R.K. Jamal, F.H. Ali, M.M. Hameed, K.A. Aadim, Designing A zener diode using Ag2O(1-X)Zno(X)/Psi structures deposited by laser induced plasma technique. Iraqi J. Sci. **61**(5), 1032–1039 (2020)

18. O.A. Ibrabim, S.K. Mustafa, R.K. Jamal, Study of the structural and optical properties of CdS prepared chemically and used as gas sensor. J. Opt. (2024). https://doi.org/10.1007/s12596-024-01782-5

19. Z. Liu, S. Nie, J. Luo, Y. Gao, X. Wang, Q. Wan, Flexible indium-tin-oxide homojunction thin-film transistors with two in-plane gates on cellulose-nanofiber-soaked papers. Adv. Electron. Mater. **5**(7), 1900235 (2019)

20. J.H. Kim et al., Flexible ITO films with atomically flat surfaces for high-performance flexible perovskite solar cells. Nanoscale **10**, 20587–20598 (2018)

21. A.E. Delahoy, S. Guo, Handbook of photovoltaic science and engineering (eds Luque, A. & Hegedus, S.), 716–796 (Wiley, New York), (2011)

22. M. Huanga, Z. Hameiria, S. Venkataraja, A.G. Aberlea, T. Mueller, Characterisation and optimisation of indium tin oxide films deposited by pulsed DC magnetron sputtering for heterojunction silicon wafer solar cell applications. Energy Procedia **33**, 91–98 (2013)

23. S.A. Yousif, H.G. Rashid, K.A. Mishji, N.F. Habubi, Design and preparation of low absorbing antireflection coatings using chemical spray pyrolysis. Int. J. Nanoelectron. Mater. **11**(4), 449–460 (2018)

24. A.H. Hasan, F.H. Ali, B.T. Chiad, Study the structural and optical properties of titanium oxide thin film, doped with chromium prepared in Sol-Gel method. Iraqi J. Phys. **16**(39), 64–70 (2018)

25. A. Feinle, M.S. Elsaesser, N. Hüsing, Sol-gel synthesis of monolithic materials with hierarchical porosity. Chem. Soc. Rev. **45**(12), 3377–3399 (2016)

26. Y. Liao, Y. Xu, Y. Chan, Semiconductor nanocrystals in sol-gel derived matrices. Phys. Chem. Chem. Phys. **15**(33), 13694–13704 (2013)

27. M.M. Mohsin, F.H. Ali, Enhancement of pigments hydrophobicity by mixing with Cr doped SiO2 nanoparticles. Chem. Methodologies **7**(5), 7335–7347 (2023)

28. W.K. Tan, H. Muto, G. Kawamura, Z. Lockman, A. Matsuda, Nanomaterial fabrication through the modification of sol-gel derived coatings. Nanomaterials **11**(1), 181 (2021)

29. D. Lončarević, Ž.D. Čupić, The perspective of using nanocatalysts in the environmental requirements and energy needs of industry. Ind. Appl. Nanomater. 91–122 (2019). https://doi.org/10.1016/B978-0-12-815749-7.00004-9

30. F.H. Ali, Hydrophilic properties of nano-structure silicate synthesis by sol-gel-dipping technique. J. Phys.: Conf. Ser. **2114**, 012076 (2021). https://doi.org/10.1088/1742-6596/2114/1/012076

31. Ruqia, A.H. Hassan Fuad, T. Ibrahim, Preparation and characterization of Ni-doped TiO2Nanostructures for surface cleaning applications. Iraqi J. Appl. Phys. **17**(1), 3–8 (2021)

32. M. Thirumoorthi, J. Thomas Joseph Prakash, Structure, optical and electrical properties of indium tin oxide ultra-thin films prepared by jet nebulizer spray pyrolysis technique. J. Asian Ceram. Soc. **4**(1), 124–132 (2016)

33. L. Dong, G.S. Zhu, H.R. Xu, X.P. Jiang, X.Y. Zhang, Y.Y. Zhao, D.L. Yan, L. Yuan, A.B. Yu, Preparation of indium tin oxide (ITO) thin film with (400) preferred orientation by sol-gel spin coating method. J. Mater. Sci.: Mater. Electron. **30**(8), 8047–8054 (2019)

34. M. Fang, A. Aristov, K.V. Rao, A.V. Kabashin, L. Belova, Particle-free inkjet printing of nanostructured porous indium tin oxide thin films. RSC Adv. **3**(42), 19501–19507 (2013)

35. H.R. Fallah, M. Ghasemia, A. Hassanzadeh, Influence of heat treatment on structural, electrical, impedance and optical properties of nanocrystalline ITO films grown on glass at room temperature prepared by electron beam evaporation. Phys. E Low-dimensional Syst. Nanostruct. **39**(1), 69–74 (2007)

36. Y.S. Jung, Spectroscopic ellipsometry studies on the optical constants of indium tin oxide films deposited under various sputtering conditions. Thin Solid Films **467**(1), 36–42 (2004)

37. J.H. Lee, Y.H. Kim, S.J. Ahn, T.H. Ha, H.S. Kim, Grain-size effect on the electrical properties of nanocrystalline indium tin oxide thin films. Mater. Sci. Eng. B **199**, 37–41 (2015)

38. M. Parthibavarman, K. Vallalperuman, S. Sathishkumar, M. Durairaj, K. Thavamani, A novel microwave synthesis of nanocrystalline SnO2 and its structural optical and dielectric properties. J. Mater. Sci.: Mater. Electron. **25**(2), 730–735 (2014)

39. H.D. Hamadalla, F.H. Ali, Preparation and characterization of metal-doped titanium dioxide nanostructures by sol-gel method. Iraqi J. Appl. Phys. **19**(4A), 49–54 (2023)

40. W.A.A. Twej, F.H. Ali, A.K. Al-Khafaji, Structural and optical properties of Al-doped TiO2 thin films prepared by dip-coating method. J. Spectrosc. Mol. Phys. **10**(10), 91–96 (2015)

41. A. Eshaghi, M. Pakshir, R. Mozaffarinia, Preparation and photo-induced superhydrophilicity of composite TiO2-SiO2-In2O3 thin film. Appl. Surf. Sci. **256**(23), 7062–7066 (2010)

42. A.P. Amalathas, M.M. Alkaisi, Effects of film thickness and sputtering power on properties of ITO thin films deposited by RF magnetron sputtering without oxygen. J. Mater. Sci. Mater. Electron. **27**(10), 11064–11071 (2016)

43. M. Thirumoorthi, J.T.J. Prakash, Structure, optical and electrical properties of indium tin oxide ultra-thin films prepared by jet nebulizer spray pyrolysis technique. J. Asian Ceram. Soc. **4**(1), 124–132 (2016)

44. M.M.H. Jafan, M.R.Z. Meymian, R. Rahimi, M. Rabbani, The effect of solvents and the thickness on structural, optical and electrical properties of ITO thin films prepared by a sol-gel spin-coating process. J. Nanostruct. Chem. **4**(1), (2014). https://doi.org/10.1007/s40097-014-0089-y

45. M.A. Marzouk, S.M. Abo-Naf, Structure characterization and photoluminescence of sol-gel synthesized AgDy-codoped silica phosphor. J. Non-Cryst. Solids **505**, 292–300 (2019)

46. J. Kim, S. Shrestha, M. Souri, J.G. Connell, S. Park, A. Seo, High-temperature optical properties of indium tin oxide thin-films. Sci. Rep. **10**, 12486 (2020)

47. Z. Xu, P. Chen, Z. Wu, F. Xu, G. Yang, B. Liu, C. Tan, L. Zhang, R. Zhang, Y. Zheng, Influence of thermal annealing on electrical and optical properties of indium tin oxide thin films. Mater. Sci. Semicond. Process. **26**(1), 588–592 (2014)

48. V. Arivazhagan, S. Rajesh, Influence of In/Sn ratio on nanocrystalline indium tin oxide thin films by spray pyrolysis method. Arch. Phy. Res. **2**(1), 19–25 (2011)

49. Q.T. Bui, I.K. Yu, A.I. Gopalan, G. Saianand, W. Kim, S.H. Choi, Facile fabrication of metal oxide based catalytic electrodes by

AC plasma deposition and electrochemical detection of hydrogen peroxide. Catalysts **9**(11), 888 (2019)

50. R.A.H. Hassan, F.T. Ibrahim, Preparation and characterization of anatase titanium dioxide nanostructures as smart and self-cleaned surfaces. Iraqi Journal Of Applied Physics **16**(4), 13–18 (2020)

51. S.Y. Khalaf, F.H. Ali, Hydrophilic properties study of Mn-TiO2 thin films deposited by dipping technique. Iraqi J. Phys. **19**(49), 62–74 (2021)

52. Y. Li, Z. Xu, S. Zhao, D. Song, B. Qiao, Y. Zhu, J. Meng, Benefits of the hydrophobic surface for CH3NH3PbI3 crystalline growth towards highly efficient inverted perovskite solar cells. Molecules **24**(10), 2027 (2019)

53. M.G. Baek, J.E. Shin, S.G. Park, Differences in ITO interface characteristics change according to the formation of aromatic-ring and aliphatic self-assembled monolayers. Crystals **11**(1), 26 (2021)

54. K. Krukiewicz, D.C. Główka, R.M. Turczyn, A.B. Grzechnik, C.V. Giraldo, K. Erfurt, A. Chrobok, J.F. Vincent, S. Pouget, D. Djurado, M.J.P. Biggs, Flexible transparent, and cytocompatible nanostructured indium tin oxide thin films for bio-optoelectronic applications. ACS Appl. Mater. Interfaces **15**(39), 45701–45712 (2023)

55. Ravichandran, J. Sahadevan, P. Sivaprakash, S. Sagadevan, I. Kim, A.M., A. Ali, S.E. Tighezza Muthu, Synthesis and physico-chemical properties of graphene incorporated indium tin oxide nanocomposites for optoelectronic device applications. Mater. Sci. Eng.: B, **301**(117199), (2024)